Original scientific paper

Integrated bio-electro-Fenton approach for efficient removal of the antiviral sofosbuvir in aqueous medium: kinetics, parameters optimization, mineralization pathway, and biodegradability enhancement

Amine Asserghine[1,2], Clément Trellu[2], Miloud El Karbane[3], Fouad Echerfaoui[3], Abdelkader Zarrouk[1,✉] and Ghizlan Kaichouh[1,✉]

[1]Laboratory of Materials, Nanotechnology and Environment (LMNE), Faculty of Sciences, Mohammed V University, PO. Box. 1014, Agdal, Rabat, Morocco
[2]Laboratoire Géomatériaux et Environnement (LGE), EA 4508, Université Gustave Eiffel, 77454 Marne-la-Vallée, Cedex 2, France
[3]Laboratory of Analytical Chemistry and Bromatology (LCAB), Faculty of Medicine and Pharmacy, Mohammed V University, Rabat, Morocco
Corresponding authors: ✉*azarrouk@gmail.com;* ✉*g.kaichouh@gmail.com;* Tel.: +212-665-201-397

Abstract

The accumulation of antiviral drugs, such as sofosbuvir (SOF), in aquatic environments raises growing concerns due to their persistence and potential ecological risks. This study addresses the need for effective degradation strategies by investigating the homogeneous electro-Fenton (EF) process in a Pt/carbon felt cell for the degradation and mineralization of SOF in an aqueous medium. A Box-Behnken design (BBD) was employed to optimize key operational parameters, including initial Fe^{2+} concentration, current intensity, and initial SOF concentration, targeting chemical oxygen demand (COD) removal as the main response. The model showed excellent predictability ($R^2 = 0.99$), and the optimal conditions were identified as 400 mA current intensity, $c_{SOF-0} = 0.1$ mM, and $c_{Fe^{2+}-0} = 0.1$ mM. Under these conditions, 97% of SOF was degraded within 5 min, while complete mineralization was achieved within 5 h. Biodegradability tests revealed an increase in the BOD_5/COD ratio to 0.41 after 2 h of electrolysis, indicating that the EF process can be effectively coupled with a biological treatment. The combined bio-electro-Fenton (bio-EF) approach successfully achieved complete mineralization, offering a cost-effective and sustainable strategy for the removal of recalcitrant pharmaceutical pollutants from water.
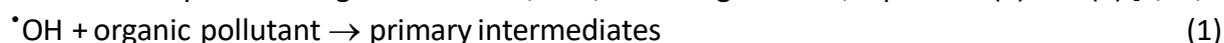
Keywords

Degradation; Box-Behnken design; hydroxyl radicals; biological treatment

Introduction

Industrial and anthropogenic activities continuously release various pollutants into aquatic environments, including surfactants, pharmaceuticals, dyes, pesticides, and phenolic compounds, many of which are toxic, persistent, and resistant to conventional treatment [1,2]. Pharmaceuticals represent a major concern as they span a wide range of therapeutic classes, including antivirals, nonsteroidal anti-inflammatory drugs (NSAIDs), β-blockers, lipid regulators, antibiotics, and anti-depressants. While essential in healthcare, their widespread and sometimes careless use leads to continuous release into water bodies [3,4]. These residues, from both human and veterinary applications, are often only partially metabolized and excreted, ultimately reaching aquatic systems through wastewater treatment plant (WWTP) discharges, which often fail to completely eradicate them. Consequently, these persistent pollutants are detected in groundwater, lakes, rivers, and even drinking water, posing risks to ecosystems and human health [5].

Among pharmaceutical pollutants, antiviral drugs have gained attention due to their role in treating infections like hepatitis, herpes, influenza, and HIV [6,7]. Recent viral outbreaks, such as swine flu and COVID-19, have further increased focus on these medications [8,9]. Their extensive use raises concerns about environmental impact. Sofosbuvir (SOF), a nucleotide polymerase inhibitor approved by the U.S. Food and Drug Administration (FDA) for chronic hepatitis C treatment [10], is effective but only partially metabolized and excreted through faeces and urine [11], leading to its presence in wastewater. Developing efficient treatment strategies for such persistent pollutants is essential to safeguarding water quality, ensuring ecological protection, and addressing an urgent public health issue [12,13].

Conventional wastewater treatment processes, including physical, chemical, and biological methods, often fail to remove persistent and toxic pollutants effectively. This has driven growing interest in advanced oxidation processes (AOPs) [13-15], which generate highly reactive species *in-situ*, capable of mineralizing non-biodegradable organic contaminants [16]. Among these species, hydroxyl radicals ($^\bullet$OH) are the primary oxidants, with a high redox potential ($E° = 2.80$ V *vs.* SHE), able to non-selectively convert organics into CO_2, H_2O, and inorganic ions, Equations (1) and (2) [1,17,18].

$$^\bullet OH + \text{organic pollutant} \rightarrow \text{primary intermediates} \tag{1}$$

$$\text{Primary intermediates} + {}^\bullet OH \rightarrow CO_2 + H_2O + \text{inorganic ions} \tag{2}$$

Various AOPs have been studied and are generally classified according to their driving force. Energy-based methods, such as photocatalysis [13], rely on light irradiation to generate reactive species. Oxidant-based methods include the activation of oxidants such as peroxymonosulfate (PMS) [19] and peroxodisulfate (PDS) [15], which produce powerful radicals upon activation. In parallel, electrochemical advanced oxidation processes (EAOPs), such as the electro-peroxone process [20], the electro-Fenton (EF) process [17], and related techniques, have gained increasing attention. EAOPs offer the advantages of *in-situ* oxidant generation and flexible operating conditions [21]. Among these, the EF process has attracted particular interest due to its high efficiency in degrading resistant organic pollutants and is therefore the main focus of this study [22].

In the EF process, Fenton's reagent, a combination of hydrogen peroxide (H_2O_2) and ferrous ions (Fe^{2+}), is electrochemically generated, with H_2O_2 formed through the two-electron oxygen reduction reaction (ORR) (Equation (3)) and Fe^{2+} produced *via* the one-electron reduction of added ferric ions (Fe^{3+}) at a suitable cathode (Equation (4)), leading to continuous formation of hydroxyl radicals ($^\bullet$OH) through the Fenton reaction (Equation (5)) [23-25].

$$O_2 + 2H^+ + 2e^- \rightarrow H_2O_2 \tag{3}$$

$$Fe^{3+} + e^- \rightarrow Fe^{2+} \tag{4}$$

$$Fe^{2+} + H_2O_2 \rightarrow Fe^{3+} + {}^\bullet OH + OH^- \tag{5}$$

Although EF has been extensively studied on synthetic effluents, the increasing occurrence of emerging micropollutants makes it important to understand how these compounds behave and whether the by-products formed are biodegradable. Studies on real effluents, whether from highly concentrated industrial sources or from wastewater treatment plants with much lower pollutant levels, have shown that it is often difficult to draw clear conclusions regarding the biodegradability of transformation products. To the best of our knowledge, no studies have investigated the degradation and mineralization of sofosbuvir. The EF process faces operational limitations such as long treatment times and high electricity consumption, which restrict its large-scale application [17]. Combining EF with biological treatment (bio-EF) can offer substantial benefits, either as a pre-treatment to partially oxidize refractory organics and enhance biodegradability, or as a post-treatment to remove residual recalcitrant pollutants, maintaining high mineralization while reducing overall costs [26,27]. The efficiency of EF depends on factors such as current intensity, pH, and catalyst and pollutant concentrations [17], and advanced experimental design and modelling approaches are often employed to optimize these parameters. Among them, artificial neural networks (ANNs) [28], reaction kinetics [29], and response surface methodology (RSM) [30] have been widely applied to predict and optimize EF outcomes. In this study, both the one-factor-at-a-time (OFAT) and design of experiments (DOE) approaches were employed to ensure consistency and correlation of the results.

This work aims to investigate the homogeneous EF degradation and mineralization of SOF in aqueous medium. A 3^3 Box-Behnken design (BBD), a widely used form of RSM, was applied to optimize key operational parameters, including initial catalyst concentration ($C_{Fe^{2+}-0}$), current intensity (I), and initial pollutant concentration (C_{SOF-0}), to maximize chemical oxygen demand (COD) removal. A quadratic regression model was developed from the experimental data to evaluate the impact of each variable on process performance. The optimal conditions were identified and used for further testing. The results from this approach were compared with those obtained from a more traditional approach (OFAT) to validate the results and ensure their reliability. Subsequently, the evolution of the BOD_5/COD ratio was assessed to determine the evolution of the biodegradability of the solution, in view of combining the EF process with a biological post-treatment (bio-EF).

Experimental

Chemicals and reagents

The chemicals used in this work were either of HPLC, analytical or reagent grade. Sofosbuvir ($C_{22}H_{29}FN_3O_9P$) was purchased from Sigma-Aldrich and used as the target pollutant. Anhydrous sodium sulphate ($Na_2SO_4 \geq 99$ % purity) and iron(II) sulphate heptahydrate ($FeSO_4 \cdot 7H_2O \geq 99$ % purity) were supplied by Merck and Sigma-Aldrich, respectively. The pH values were adjusted using sulfuric acid ($H_2SO_4 \geq 96$ % purity) and sodium hydroxide (NaOH) from Acros Organics™ and Fluka, respectively. To ensure consistency and reliability in the experiments, all solutions were prepared with ultra-pure water produced by a Millipore Milli-Q® (simplicity 185) system, with a resistivity > 18 MΩ cm at 25 °C.

Electrochemical system

The homogeneous EF experiments were conducted in a 250 mL undivided cylindrical glass open cell (ϕ = 7 cm), equipped with three electrodes at 20±1 °C. The anode used was a platinum (Pt) electrode (2.5×2 cm), while the cathode was a three-dimensional carbon felt (CF) electrode

(6×5×0.5 cm) from Carbon-Lorraine (Paris, France). The electrodes were positioned facing each other in parallel, 1.5 cm apart. The third electrode, a saturated KCl calomel electrode, served as the reference electrode and was immersed directly in the solution (Figure 1). SOF was introduced with $FeSO_4 \cdot 7H_2O$ as the catalyst and Na_2SO_4 (0.05 M) as the supporting electrolyte. The initial pH of SOF solutions was measured using a CyberScan pH 110 pH meter from Eutech Instruments and was adjusted to 3±0.1, using H_2SO_4, the optimal value for the EF process [17,24,31]. To ensure saturated oxygen conditions for H_2O_2 production, compressed air was bubbled at a rate of 1 L min^{-1}, initiated 10 min prior to the start of each experiment and maintained throughout the electrolysis process. Continuous magnetic stirring at 400 rpm facilitated mass transport from/towards the electrode surfaces. the electrochemical cell was powered by a Potentiostat/Galvanostat PGZ100 from Voltalab Instrument. Experiments were conducted under constant current (100 to 500 mA), with samples collected at pre-set time intervals to evaluate degradation and mineralization concentrations.
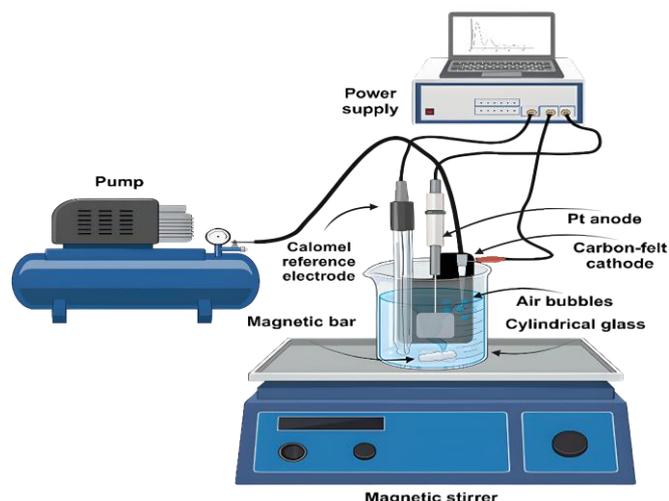

Figure 1. *An open and undivided lab-scale, three-electrode reactor fed with compressed air for operating the EF process in batch mode*

Biological treatment

The biological treatment was performed in batch mode, under aerobic conditions, using activated sludge collected from a nearby wastewater treatment plant in Ain El-Aouda (Rabat, Morocco), without prior purification. The culture medium, prepared in a 250 mL Erlenmeyer flask at 20±1 °C, contained 200 mL of EF-treated C_{SOF-0} = 0.1 mM solution for 2 h. Mineral supplements were added to the flask: 33.4 mg L^{-1} Na_2HPO_4, 43.8 mg L^{-1} KH_2PO_4, 27.5 mg L^{-1} $CaCl_2$, 22.5 mg L^{-1} $MgSO_4 \cdot 7H_2O$ and 3 mg L^{-1} NH_4NO_3. After adjusting the pH to 7±0.2 with NaOH, trace elements were introduced: 1.36 mg L^{-1} $FeSO_4 \cdot 7H_2O$, 0.24 mg L^{-1} $CuSO_4 \cdot 2H_2O$, 0.25 mgL^{-1} $ZnSO_4 \cdot 5H_2O$, 0.11 mg L^{-1} $NiSO_4 \cdot 6H_2O$ and 1.01 mg L^{-1} $MnSO_4 \cdot H_2O$. The flask was then inoculated with 0.5 g L^{-1} of activated sludge, stirred for 3 weeks, and covered with a cotton plug to ensure proper oxygenation [32-34]. Each day for 21 days, 5 mL aliquots were collected and filtered with a 0.45 µm filter for further COD analysis.

Instruments and analytical procedures

High-performance liquid chromatography (HPLC)

The degradation kinetics of SOF were analysed using high-performance liquid chromatography (HPLC) on a Thermo Scientific Dionex UltiMat 3000 system, equipped with a PhotoDiode Array (PDA) detector. Separation was conducted on a reversed-phase Hypersil BDS C18 column (150×4.6 mm, 5 µm) at 30 °C. Isocratic elution was used with a mobile phase composed of a mixture of (water +

+ 0.1 % H_3PO_4) / acetonitrile (55:45 v/v). The mobile phase was pumped at a flow rate of 1 mL min^{-1}, with an injection volume set at 50 μL, and detection was performed at a wavelength of λ = 260 nm, revealing a distinct retention peak at t_R = 5.06 min.

Chemical oxygen demand

The chemical oxygen demand (COD) was determined using the potassium dichromate assay with an RD 125 thermoreactor (Lovibond®). Samples were mixed with H_2SO_4, mercury(II) sulphate ($HgSO_4$), and potassium dichromate ($K_2Cr_2O_7$) in vials and incubated for 2 h at 150 °C in the thermoreactor [35]. After cooling, COD values were measured using a Photometer (Lovibond® MD 200 COD VARIO). All experiments were conducted at 20±1 °C for accuracy.

Instantaneous current efficiency

The instantaneous current efficiency (ICE, %) defined as the fraction of the applied current to oxidize organic compounds, was calculated using Equation (6) to understand better the impact of current on mineralization efficiency of aqueous SOF *via* the EF process [24,36,37].

$$\text{ICE} = \frac{(\text{COD}_t \text{-COD}_{t+\Delta t})FV_s}{8I\Delta t}100 \tag{6}$$

where COD_t and $\text{COD}_{t+\Delta t}$ are the COD, g O_2 L^{-1} values at times t / s and $t + \Delta t$ / s, F is the Faraday constant (96,487 C mol^{-1}), V_s / L is the volume of the treated solution, the constant 8 is the oxygen equivalent mass (g eq^{-1}), and I / A is the applied current.

Energy consumption

The energy consumption (EC, kWh (g COD)$^{-1}$) for each experiment, expressed per unit mass of COD removed, was calculated using Equation (7). Measurement of energy consumption is crucial for evaluating the electrochemical process and estimating operational treatment costs [24,37,38].

$$\text{EC} = \frac{E_{\text{cell}}It}{\Delta\text{COD}_t V_s} \tag{7}$$

where E_{cell} / V is the average cell voltage, I / A is the applied current, ΔCOD_t is the decay of COD at time t, V_s / L is the volume of the treated solution, and t / h is the electrolysis time.

Biological oxygen demand

The biological oxygen demand (BOD) was used to measure the progression of solution biodegradability. The measurements were conducted using the OxiDirect system (Lovibond®), with the 5-day respirometry method. The bottles were continuously stirred and incubated in a TC 135 S thermostat cabinet (Lovibond®) at 20±1 °C, under dark conditions. An inoculum was obtained from a nearby WWTP, and N-allylthiourea (ATH) was added as a nitrification inhibitor in each bottle, and the pH was carefully adjusted to remain between 6.5 and 7.5. Each bottle contained a rubber sleeve with 4 drops of 45 % KOH to absorb CO_2 generated during respiration [27].

Box-Behnken experimental design

Response surface methodology is a statistical approach for designing experiments, analysing factor interactions, and optimizing processes while minimizing the number of trials [39,40]. In this study, a 3^3 Box-Behnken experimental design (BBD) was used to optimize experimental parameters with fewer tests. The two main variables affecting SOF mineralization effectiveness were selected: X_1 - current applied and X_3 - initial catalyst concentration, $C_{Fe^{2+}\text{-}0}$ / mM. Another variable was taken into consideration, X_2 - initial sofosbuvir concentration, $C_{SOF\text{-}0}$ / mM, which might change depending

on the nature of the pollutant. The BBD represents a factorial plane at 3 levels: low, middle, and high (-1, 0, 1). The coded and actual values are shown in Table 1.

Table 1. *The levels studied for each factor in the 3^3 Box-Behnken design*

Coded factors	Variable	Coded levels		
		-1	0	1
		Actual values		
X_1	I / A	200	300	400
X_2	C_{SOF-0} / mM	0.10	0.15	0.20
X_3	$C_{Fe^{2+}-0}$ / mM	0.05	0.10	0.15

The total number of experiments needed can be calculated using the following Equation (8):

$$N = 2k(k\text{-}1) + C_0 \tag{8}$$

where N, k, and C_0 correspond to the number of experiments, independent variables, and central points, respectively. It resulted in 15 tests being carried out using three central points.

The response variable was the mineralization effectiveness, calculated as follows (Equation 9) [41]:

$$\text{COD removal} = \frac{\text{COD}_0 - \text{COD}_t}{\text{COD}_0} 100 \tag{9}$$

where COD_0 and COD_t correspond to the value of the COD at t_0 and at time t, respectively.

The quadratic response model can be described as shown in Equation (10), which includes linear terms, square terms, and interactions between factors.

$$Y = \beta_0 + \sum_{j=1}^{k}\beta_j X_j + \sum_{j=1}^{k}\beta_{jj}{X_j}^2 + \sum_{i}^{k}\sum_{j}\beta_{ij}X_i X_j + \varepsilon \quad (i < j) \tag{10}$$

where Y is the predicted response, ε represent the experimental error, β_0, β_j, β_{jj} and β_{ij}, are the regression coefficients for intercept, linear, quadratic, and interaction terms, respectively, while X_i and X_j are the coded variables.

The experimental response obtained with the BBD was characterized by a quadratic polynomial model (Equation (11)):

$$Y = \beta_0 + \beta_1 X_1 + \beta_2 X_2 + \beta_3 X_3 + \beta_{11}X_1^2 + \beta_{22}X_2^2 + \beta_{33}X_3^2 + \beta_{12}X_1X_2 + \beta_{13}X_1X_3 + \beta_{23}X_2X_3 + \varepsilon \tag{11}$$

After the regression of the experimental data, analysis of variance (ANOVA) was conducted to assess the reliability and significance of the fitted model, considering lack of fit, the coefficient of determination (R^2), and the model's overall adequacy, using Design-Expert software (DX13). Subsequently, 3D graphs were plotted to visualize the response surface, the interaction between factors, and their overall impact on treatment performance. Additionally, a Pareto chart and a normal plot of standardized effects were generated using Minitab statistical software version 21 to evaluate the influence of each parameter on the process.

Results and discussion

Effect of operating parameters on sofosbuvir degradation and mineralization

Effect of applied current intensity

The efficiency of electrochemical oxidation processes is fundamentally influenced by the applied current intensity (I) (Figure 2), which directly impacts the generation rate of the Fenton's reagent, and therefore the generation rate of hydroxyl radicals ($^{\bullet}$OH) through the Fenton's reaction (Equation (5)).
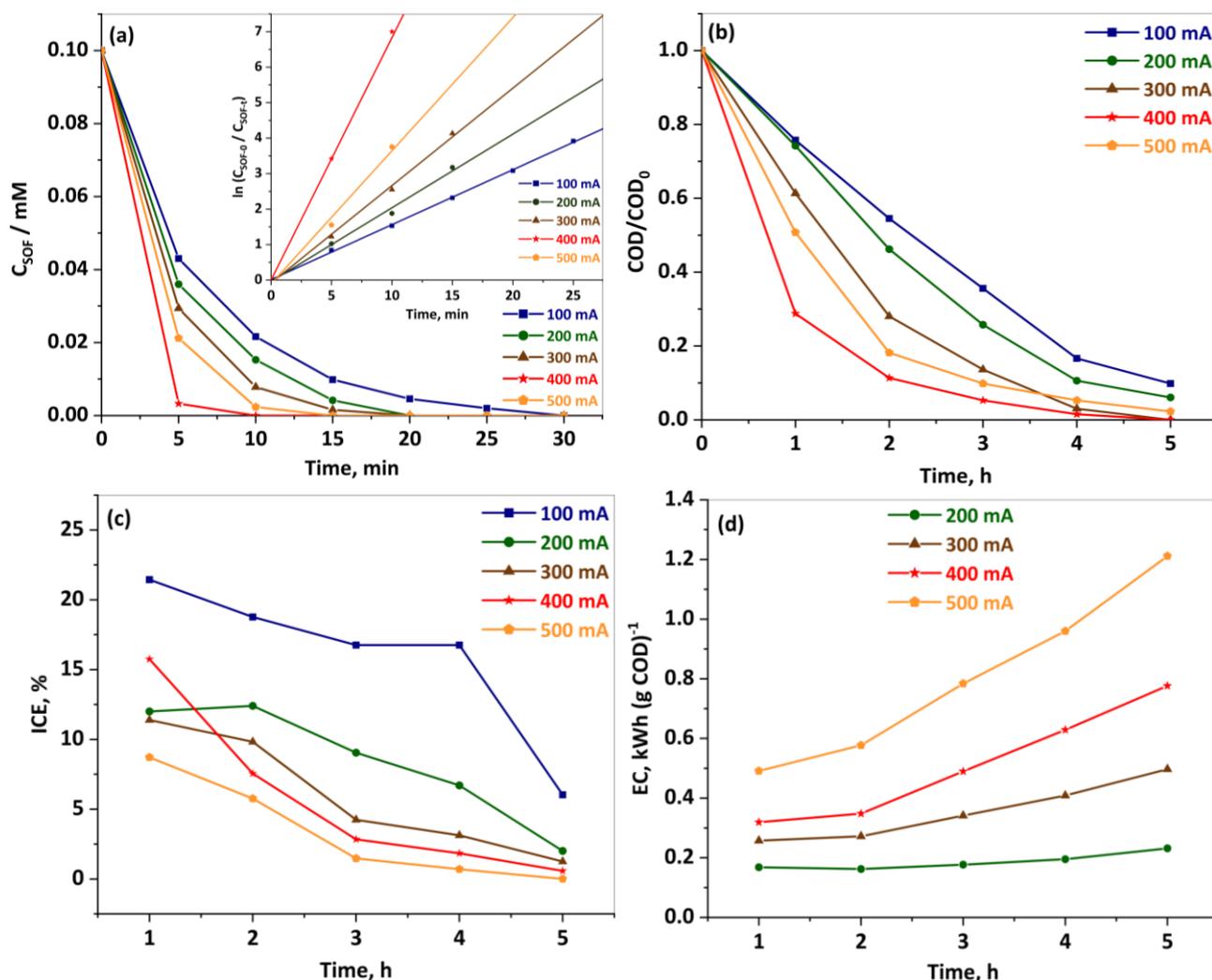
Figure 2. *Effect of applied current intensity on: (a) degradation, with the inset panel presenting the corresponding oxidation kinetics analysis, (b) mineralization, (c) instantaneous current efficiency (ICE), and (d) energy consumption (EC) during SOF removal via the EF process at pH 3±0.1; $C_{SOF\text{-}0}$ = 0.1 mM; $C_{Fe^{2+}\text{-}0}$ = 0.1 mM; V_s = 200 mL; $C_{Na_2SO_4}$ = 0.05 M*

To treat aqueous SOF solutions, the EF process was applied under controlled current electrolysis conditions, with initial concentrations of $C_{Fe^{2+}\text{-}0}$ = 0.1 mM and $C_{SOF\text{-}0}$ = 0.1 mM at pH 3±0.1. The impact of varying the applied current on the degradation kinetics of SOF was studied across different current intensities, *i.e.* 100, 200, 300, 400 and 500 mA. As shown in Figure 2a, SOF concentration dropped to zero at all current levels, with the oxidation rate increasing as the current was raised. Specifically, increasing the current from 100 to 400 mA significantly enhanced the SOF degradation rate, rising from 57 to 97 % within just 5 min of electrolysis. Consequently, the time required for >99 % degradation decreased from 30 min at 100 mA to 11 min at 400 mA. Beyond this point, the primary organic compounds remaining in the solution were aromatic by-products and short-chain carboxylic acids [31]. However, increasing the current beyond 400 mA slowed the degradation of SOF.
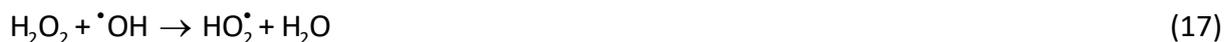
The mineralization of aqueous SOF solutions required longer treatment times. The difference between degradation and mineralization kinetics highlights the accumulation of degradation by-products in the solution. Regarding the influence of the applied current, a similar pattern was observed for both the degradation and mineralization of aqueous SOF solutions (Figure 2b). As the current intensity increased from 100 to 400 mA, the COD decreased correspondingly. At 100 mA, a 90 % mineralization rate was observed, while at 400 mA, >99 % mineralization was achieved after

5 h. However, increasing the applied current to 500 mA slowed the rate of SOF mineralization, achieving only 98 % after 5 h of electrolysis, indicating that complete oxidation at higher currents requires a longer electrolysis time. This enhancement in both degradation and mineralization is due to the increased production of H_2O_2 from Equation (3) and the regeneration of Fe^{2+} at the cathode (Equation (4)). leading to the generation of larger amounts of hydroxyl radicals ($^\bullet OH$) from Fenton's reaction (Equation (5)), thereby enhancing treatment effectiveness [34,42-44]. Equation (12) illustrates the dependence of $^\bullet OH$ generation on the concentrations of Fe^{2+} and H_2O_2 [36,43,45].

$$C_{^\bullet OH} = \lambda \left(\frac{dC_{^\bullet OH}}{dt} \right) = \lambda k C_{Fe^{2+}} C_{H_2O_2} \tag{12}$$

where λ / min is the average life span of the hydroxyl radical, $C_{Fe^{2+}\text{-}0}$ / mM and $C_{H_2O_2}$ / mM are the concentrations of ferrous ion and hydrogen peroxide, respectively, and k / (mmol L^{-1})$^{-1}$ min^{-1} is the second-order rate constant of Equation (5).

However, the decrease in treatment efficiency at higher currents may be due to secondary parasitic reactions including (i) the four-electron reduction of O_2 (Equation (13)), which hinders H_2O_2 formation (Equation (3)); (ii) H_2 evolution at the cathode (Equation (14)); and (iii) the oxidative/reductive decay of H_2O_2 at both the anode (Equation (15)) and the cathode (Equation (16)), all of which negatively impact the oxidation process. Additionally, exceeding the optimal current can accelerate the rate of $^\bullet OH$ production (Equation (17)), further complicating the process [17]. Therefore, the optimal current for both degradation and mineralization is 400 mA.

$$O_{2(g)} + 4H^+ + 4e^- \rightarrow 2H_2O \tag{13}$$

$$2H^+ + 2e^- \rightarrow H_{2(g)} \tag{14}$$

$$H_2O_2 \rightarrow O_{2(g)} + 2H^+ + 2e^- \tag{15}$$

$$H_2O_2 + 2H^+ + 2e^- \rightarrow 2H_2O \tag{16}$$

$$H_2O_2 + {}^\bullet OH \rightarrow HO_2^\bullet + H_2O \tag{17}$$

The degradation of SOF follows an exponential pattern at all applied currents, indicating a first-order reaction kinetics for its oxidation by $^\bullet OH$ (Equation (18)) [46]. This observation is supported by the apparent rate constants (k_{app}) presented in Table 2.

$$SOF + {}^\bullet OH \rightarrow \text{oxidation products} \tag{18}$$
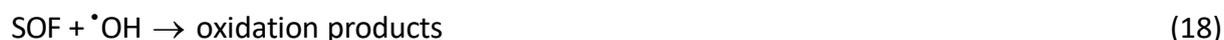
Under the steady-state approximation for $^\bullet OH$ in the EF treatment, the oxidation rate of SOF can be expressed as follows (Equation (19)) [47,48]:

$$-\frac{dC_{SOF}}{dt} = k_{abs} C_{^\bullet OH} C_{SOF} = k_{app} C_{SOF} \tag{19}$$

where k_{abs} and k_{app} represent the absolute and apparent rate constants of SOF oxidation by $^\bullet OH$, respectively.

Yielding the following expression after integration (Equation (20)) [44]:

$$\ln\left(\frac{C_{SOF-0}}{C_{SOF-t}} \right) = K_{app} t \tag{20}$$

where C_{SOF-0} and C_{SOF-t} are the concentrations of sofosbuvir at t_0 and at time t, respectively.

The kinetic constant data provide a quantitative assessment of the trends previously observed in the degradation curves. The apparent rate constants for SOF oxidation were determined from

plotting $\ln(C_{SOF-0} / C_{SOF-t})$ against time at various applied currents (Figure 2a, inset) and summarized in Table 2 alongside half-life times ($t_{1/2}$).

Table 2. *Apparent rate constant (k_{app}) and half-life times ($t_{1/2}$) for the oxidation of SOF by $^{\bullet}OH$ at different applied currents under operating conditions of Figure 2 fitted by a first-order kinetic model*

I / mA	k_{app} / min^{-1}	R^2	$t_{1/2}$ / min
100	0.15	0.999	4.5
200	0.21	0.993	3.3
300	0.27	0.996	2.5
400	0.70	0.999	1.0
500	0.38	0.990	1.9

The results confirm the acceleration of degradation with increasing current up to 400 mA, beyond which kinetics slow down despite higher energy consumption. As an alternative approach to evaluating the impact of current on the electrochemical mineralization of SOF, we calculated the ICE based on Equation (6). The results depicted in Figure 2c demonstrate that the highest ICE was achieved at lower applied currents, with a general decrease in ICE over time. Notably, ICE decreases as the applied current increases, reaching its lowest at 500 mA. This can be attributed to the increase in parasitic reactions, such as the oxidation of H_2O into O_2 (Equation (21)) and the reduction of H^+ into H_2 (Equation (14)). For all the current intensities, the highest ICE is observed at the beginning of electrolysis, after which it gradually declines. The decrease in ICE could result from (i) the generation of more stable substances, like short-chain carboxylic acids, which are more resistant to oxidation; (ii) the increase of mass transport limitations related to the short lifespan of hydroxyl radicals, since the concentration of organic compounds in the solution gradually decreases [49-51].

$$2H_2O \rightarrow O_{2(g)} + 4H^+ + 4e^- \tag{21}$$

The evaluation of energy consumption was conducted to determine the feasibility of the EF process for industrial use, as it is crucial for assessing its cost efficiency. Figure 2d illustrates how EC, calculated using Equation (7), varies with current intensities between 200 and 500 mA. The outcomes are presented in terms of kWh per gram of COD removed, over electrolysis time, h. Similarly, to ICE, the rise in EC correlates with both the applied current and the treatment time during the electrolysis of the SOF solution. Compared to ICE, increasing the current intensity has an additional adverse effect on EC, which is related to the increase of the cell potential (*i.e.* 5.7 V at 200 mA and 12.8 V at 500 mA after 1 h) that further increases the EC. Higher currents, such as 400 and 500 mA, result in significantly greater energy consumption (0.78 and 1.20 kWh (g COD)$^{-1}$, respectively) compared to lower currents like 200 and 300 mA (0.23 and 0.50 kWh (g COD)$^{-1}$, respectively). From an energy optimization standpoint, using lower currents is more efficient as it consumes less energy over time. However, selecting the appropriate current should ideally balance energy consumption with the process's effectiveness. Therefore, a current of 400 mA was identified as the optimal choice for combination with a cost-effective biological method. In this context, the bio-electro-Fenton process aims at reducing the required treatment time by EF to achieve a more energy-efficient approach for treating persistent pollutants [52].

Effect of the initial catalyst concentration

The initial concentration of ferrous ions (Fe^{2+}) is also considered a critical parameter in evaluating the efficiency of the EF process [17,53,54]. The catalytic performance of Fe^{2+} is primarily influenced by the solution's pH. At pH 3±0.1, the Fe^{2+} concentration in the reaction medium reaches its highest level,

leading to the most efficient Fenton's reaction rate (Equation (5)) [24,55]. To investigate the effect of the initial catalyst concentration on SOF mineralization and degradation, Fe^{2+} concentrations ranging from 0.05 to 0.15 mM were examined, with an optimal current of 400 mA (Figure 3).
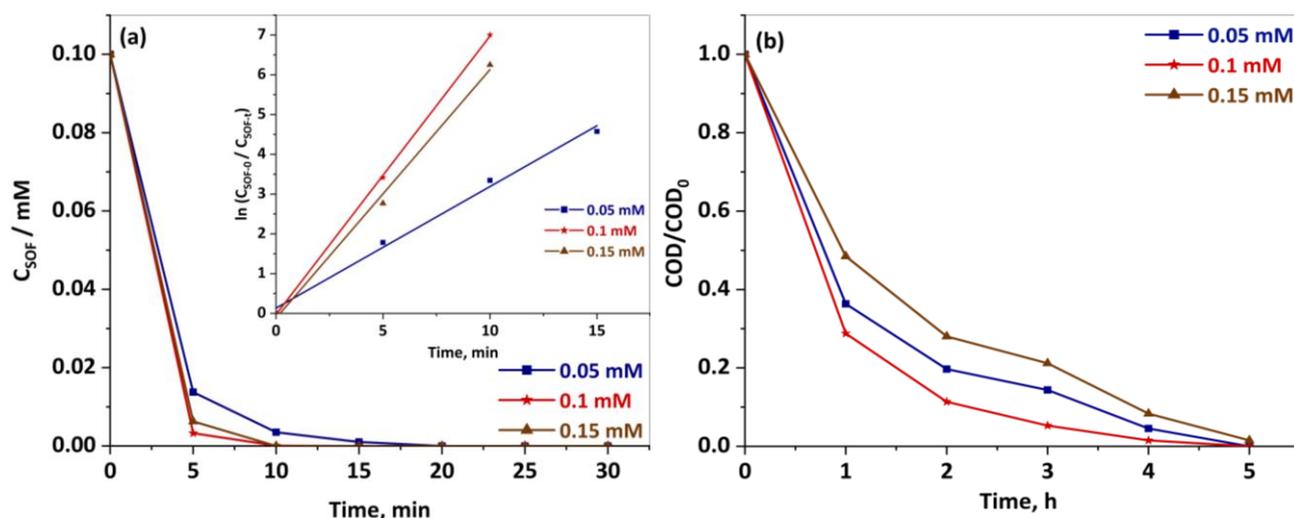

Figure 3. *Influence of the initial Fe^{2+} concentration during: (a) degradation, with the inset panel presenting the corresponding oxidation kinetics analysis, (b) mineralization on SOF removal via EF process at pH 3±0.1; C_{SOF-0} = 0.1 mM; I = 400 mA; V_s = 200 mL; $C_{Na_2SO_4}$ = 0.05 M*

The effect of $C_{Fe^{2+}-0}$ on SOF degradation revealed a significant impact on process efficiency, as shown in Figure 3a. At $C_{Fe^{2+}-0}$ = 0.05 mM, 86 % of SOF was degraded within the first 5 min, indicating that this lower Fe^{2+} concentration was insufficient to efficiently catalyse Fenton's reaction (Equation (5)) [17]. Doubling the initial ferrous iron (Fe^{2+}) concentration to 0.1 mM significantly improved the degradation efficiency to 97 % within the same timeframe of treatment, attributed to the high generation of $^{\bullet}OH$ in the bulk solution *via* Fenton's reaction (Equation (5)) [45,56,57]. However, when $C_{Fe^{2+}-0}$ was raised to 0.15 mM, the efficiency reduced to 92 % after 5 min of electrolysis. This decrease is likely due to the enhanced rate of wasting reaction (Equation (22)) [17,34,56,58], which reduces the oxidation efficiency of the process. As shown in the inset panel of Figure 3a, the degradation kinetics follow a pseudo-first-order reaction, with the k_{app} increasing up to 0.1 mM before declining at higher Fe^{2+} concentrations (Table 3).

Table 3. *Apparent rate constant (k_{app}) and half-life times ($t_{1/2}$) for the oxidation of SOF by $^{\bullet}OH$ at different catalyst concentrations under operating conditions of Figure 3, fitted by a first-order kinetic model*

$C_{Fe^{2+}-0}$ / mM	k_{app} / min^{-1}	R^2	$t_{1/2}$ / min
0.05	0.31	0.993	2.3
0.10	0.70	0.999	1.0
0.15	0.63	0.996	1.1

The mineralization of SOF (Figure 3b) exhibited notable variation with Fe2+ concentration, increasing from 95 % at 0.05 mM to 98 % at 0.1 mM, but then decreasing to 92 % at 0.15 mM after 4 h of electrolysis. These results indicate that $C_{Fe^{2+}-0}$ = 0.1 mM is optimal, providing the right balance between effective hydroxyl radical production and minimizing side reactions (Equation (22)). Therefore, this concentration was selected for subsequent experiments related to the bio-electro-Fenton process.

$$Fe^{2+} + {}^{\bullet}OH \rightarrow Fe^{3+} + OH^{-} \tag{22}$$

Effect of the initial sofosbuvir concentration

The mineralization and degradation efficiency of EAOPs is highly influenced by the initial load of organic pollutants. To better understand its impact on EF performance, electrolysis experiments were conducted at three different SOF concentrations (*i.e.* 0.1, 0.15 and 0.2 mM) under optimal conditions (Figure 4).
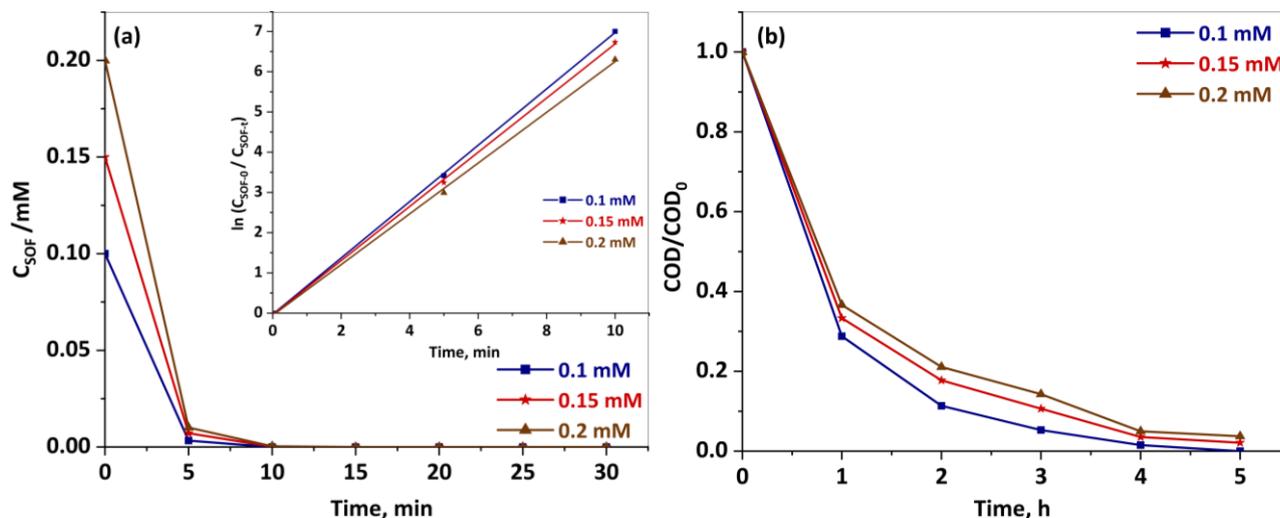

Figure 4. *Influence of initial SOF concentration during: (a) degradation, with the inset panel presenting the corresponding oxidation kinetics analysis, (b) mineralization by the EF process at pH 3±0.1; $C_{Fe^{2+}-0}$ = 0.1 mM; I = 400 mA; V_s = 200 mL; $C_{Na_2SO_4}$ = 0.05 M*

The results presented in Figure 4a and Table 4 show that the degradation yield of SOF was still very high after only 5 min of treatment when the concentration of SOF was increased from 0.1 to 0.2 mM.

Table 4. *Apparent rate constant (k_{app}) and half-life times ($t_{1/2}$) for the oxidation of SOF by $^•OH$ at different SOF concentrations under operating conditions of Figure 4, fitted by a first-order kinetic model*

C_{SOF-0} / mM	k_{app} / min^{-1}	R^2	$t_{1/2}$ / min
0.1	0.70	0.999	1.0
0.15	0.67	0.999	1.0
0.2	0.63	0.999	1.1

These results mean that a larger amount of SOF was degraded during the experiment at 0.2 mM. As these experiments were performed under mass transport limitation, the increase of SOF concentration promotes the reaction of SOF with hydroxyl radicals [34,59]. A similar pattern was observed for mineralization Figure 4b.

Optimization of COD removal

Statistical analysis

The efficiency of the EF process is influenced by various parameters, such as the initial catalyst concentration $C_{Fe^{2+}-0}$, the applied current (*I*), and the initial SOF concentration C_{SOF-0}. To optimize these factors, we used the BBD with the analysis time fixed at 4 h. This study involved 15 experiments, as determined using Equation (8). The variables considered in the experiments, along with the results from the BBD, including the observed and predicted COD removal efficiencies for SOF in the EF process, are presented in Table 5.

Table 5. *The 3^3 Box-Behnken experimental matrix for different factors influencing SOF removal in the EF process, along with the observed and predicted COD values*

Run	Actual variables			COD removal, %	
	I / mA (X_1)	C_{SOF-0} / mM (X_2)	$C_{Fe^{2+}-0}$ / mM (X_3)	Observed	Predicted
1	200	0.15	0.15	88.5	88.3
2	300	0.20	0.05	92.0	91.9
3	400	0.15	0.05	96.1	96.3
4	200	0.20	0.10	89.3	89.4
5	300	0.10	0.05	92.5	92.4
6	400	0.10	0.10	98.5	98.4
7	300	0.20	0.15	90.2	90.3
8	200	0.15	0.05	87.3	87.4
9	400	0.20	0.10	95.3	95.3
10	300	0.10	0.15	92.8	93.0
11	300	0.15	0.10	91.3	91.1
12	300	0.15	0.10	90.9	91.1
13	300	0.15	0.10	91.0	91.1
14	200	0.10	0.10	89.4	89.4
15	400	0.15	0.15	94.5	94.4

To validate the statistical model, we conducted an ANOVA analysis, as summarized in Table 6. This assessment focused on mean square ratios, *F*-values, and *p*-values, where a *p*-value below 0.05 indicates the significance of the model at a 95 % confidence level [60].

Table 6. *Analysis of variance (ANOVA) results for the quadratic model of operational parameters in SOF removal via the EF process*

Source	Sum of squares	Degree of freedom	Mean square	*F*-value	*p*-value	
Model	130.85	9	14.54	342	< 0.0001	Significant
A^a: I	111.30	1	111.30	2619	< 0.0001	
B^b: C_{SOF-0}	5.10	1	5.10	120	0.0001	
C^c: $C_{Fe^{2+}-0}$	0.4950	1	0.4950	11.6	0.0190	
AB	2.53	1	2.53	59.5	0.0006	
AC	2.02	1	2.02	47.5	0.0010	
BC	1.16	1	1.16	27.2	0.0034	
A^2	2.94	1	2.94	69.3	0.0004	
B^2	4.93	1	4.93	116	0.0001	
C^2	0.4512	1	0.4512	10.6	0.0225	
Residual	0.2125	5	0.0425			
Lack of fit	0.1608	3	0.0536	2.08	0.3416	Not significant
Pure error	0.0517	2	0.0258			
Corr. total^d	131.06	14				

[a]$A = X_1$; [b]$B = X_2$; [c]$C = X_3$; [d]Corrected total sum of squares.

The results confirm the model's statistical significance, with a very low *p*-value (<0.0001) underscoring its robustness. In addition, the terms *A*, *B*, *C*, *AB*, *AC*, *BC*, A^2, B^2 and C^2 showed statistical significance (p < 0.05), demonstrating the model's reliability. The positive signs of variables such as X_1, X_1^2 and X_2^2 indicate that they positively affect SOF mineralization. Conversely, the negative signs of X_2, X_3, and the interaction terms X_1X_2, X_1X_3, X_2X_3 and X_3^2 suggest a negative impact (Figure 6b). Consequently, the quadratic polynomial model that represents the correlation between these variables and COD removal is given by Equation (23):

$$\text{COD removal} = 91.07 + 3.73X_1 - 0.80X_2 - 0.25X_3 - 0.80X_1X_2 - 0.71X_1X_3 - 0.54X_2X_3 +$$
$$+ 0.89X_1^2 + 1.16X_2^2 - 0.35X_3^2 \tag{23}$$

Furthermore, the high *F*-values obtained further validate the model, indicating that the variability in each parameter is substantial compared to the error variance [61]. The fact that there is only a 0.01 % chance of obtaining such a large *F*-value due to noise underscores the model's significance and robustness. The *F*-values also reveal the effect of different factors on the process, with the following sequence of significance: $I > C_{SOF-0} > C_{Fe^{2+}-0}$. These findings highlight the crucial role of each parameter in determining process efficiency. Moreover, the lack of fit (LOF) test serves to verify the alignment between the model and the observed data [62]. In this case, the LOF value of 2.08 is statistically insignificant compared to the pure error. There is a 34.2 % chance that such *F*-value for a lack of fit could occur due to noise. These results validate the strong agreement between the experimental data and the model, suggesting a good fit.

Table 7. Fit quality results based on ANOVA analysis for SOF mineralization

Fit quality indicators	Fit values
Standard deviation	0.206
Mean	91.97
CV, %	0.224
R^2	0.998
R_{adj}^2	0.996
R_{pred}^2	0.980
Adequate precision	65.47
PRESS[a]	2.690

[a]Predicted residual error sum of squares

The model's accuracy is reflected in the coefficient of determination (R^2), with a value of 0.998, demonstrating that only 0.2 % of the total variation remains unexplained by the quadratic regression model. This is closely supported by the adjusted R^2 = 0.996, as presented in Table 7, highlighting the model's robustness in fitting the experimental data and its predictive reliability [63]. The predicted R^2 = 0.98 aligns closely with the adjusted R^2, with a difference of less than 0.1, further demonstrating the model's high accuracy. The strong alignment between the predicted and experimental values underscores the model's effectiveness and accuracy in predicting the COD removal of SOF. Figure 5 reveals that all data points align closely with a straight line, further validating the model's suitability for process prediction and optimization.
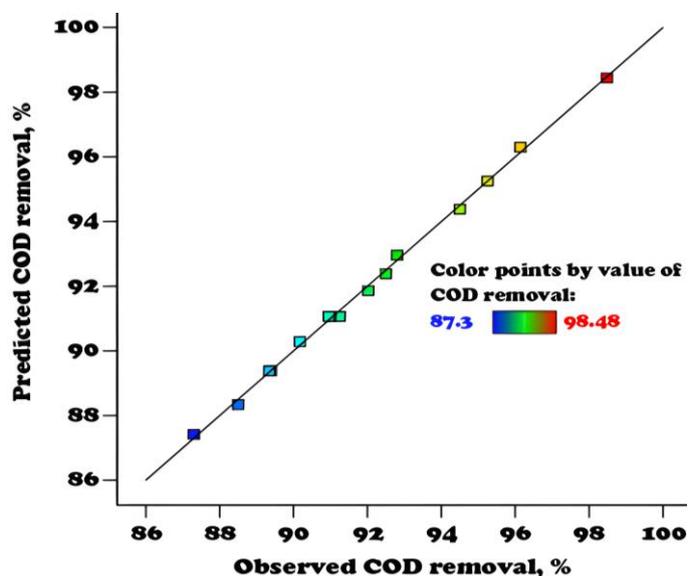

Figure 5. Linear correlation of actual versus predicted values for SOF removal via the EF process

The "Adequate precision" evaluates the ratio of signal-to-noise, where values above 4 are considered desirable [61,62]. In this study, the ratio of 65.47 indicates a strong signal relative to noise, confirming the model's reliability and suitability for exploring the design space. In addition, the coefficient of variation (CV) measures the degree of variation in the data, with lower values indicating better reproducibility. In this case, the CV value of 0.224 % signifies excellent reproducibility [63]. Furthermore, to assess the model's predictive accuracy, the predicted residual sum of squares (PRESS) is used to evaluate how well the model fits each point in the design. A PRESS ratio of 2.69 was obtained, indicating a good fit. Generally, lower PRESS values suggest better predictive ability.

Pareto analysis

The Pareto diagram reveals the extent to which each parameter and its interactions affect the response. This is determined using Equation (24) [64,65]:

$$P_i = \frac{\beta_i^2}{\sum \beta_i^2} 100 \quad (i \neq 0) \tag{24}$$

where P_i indicates the percentage contribution of factor X_i to the overall variability, and β_i refers to the coefficient associated with factor X_i.

The Pareto chart in Figure 6a illustrates the influence of each factor in terms of content, including their squared terms and interactions.
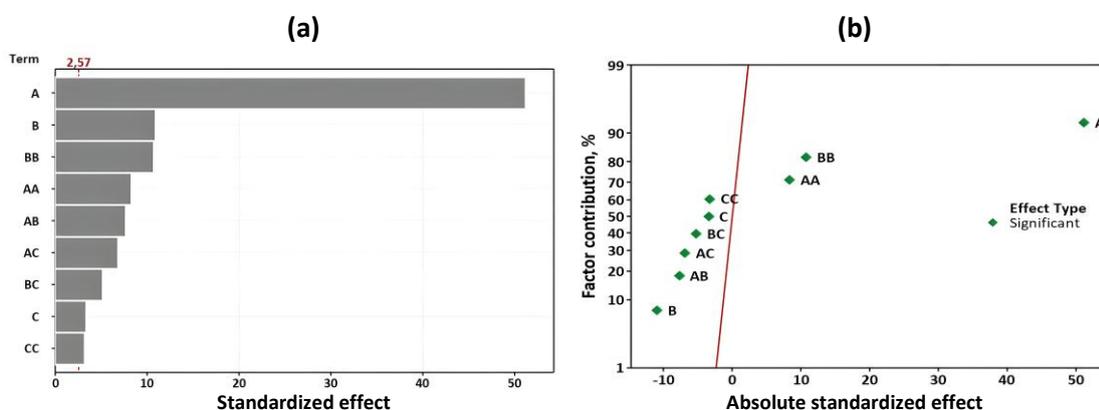

Figure 6. (a) Pareto chart of standardized effects at 0.05 confidence level (2.57 reference line); (b) normal plot of standardized effects for assessing the significance of variables on SOF removal

The chart features horizontal bars with a red vertical reference line marking statistical significance. Factors with bars crossing this line are considered to have a significant statistical impact at a 0.05 significance threshold. The diagram reveals that all three factors significantly affect COD removal of SOF, with current intensity (*I*) having the greatest effect, followed by the initial sofosbuvir concentration C_{SOF-0}, and then the initial catalyst concentration $C_{Fe^{2+}-0}$. Additionally, interactions between these factors and their squared terms also affect COD removal. Figure 6b presents the normal plot of standardized effects, where factors further from zero indicate greater statistical significance. The main factors are significant at the 0.05 threshold, along with their interactions and quadratic terms. The plot also reveals the direction of each effect, offering further insights. For instance, the applied current (*A*) exhibits a positive standardized effect, meaning that as the applied current rises from 200 to 400 mA, COD removal increases. In contrast, initial SOF concentration (*B*) shows a negative standardized effect, indicating that higher concentrations lead to a reduction in COD removal. Additionally, the quadratic terms for current (A^2) and concentration of SOF (B^2) also have positive effects. Meanwhile, the remaining interactions and terms exhibit negative effects.

Overall, the plot provides a clear view of the significant factors and their influence on the COD removal process.

Interactions between process variables

The 3D surface plots serve to visualize interactions among variables and help determine optimal conditions. These plots show how two independent variables influence the selected response, with the third variable held constant. Figure 7 presents the most relevant fitted response surface plots, illustrating COD removal as a function of significant variables and showing how two factors influence SOF mineralization *via* the EF process, with the third factor held constant at its optimal value. The plots reveal clear peaks, which identify the optimal regions for the analysed factors and their highest response values.
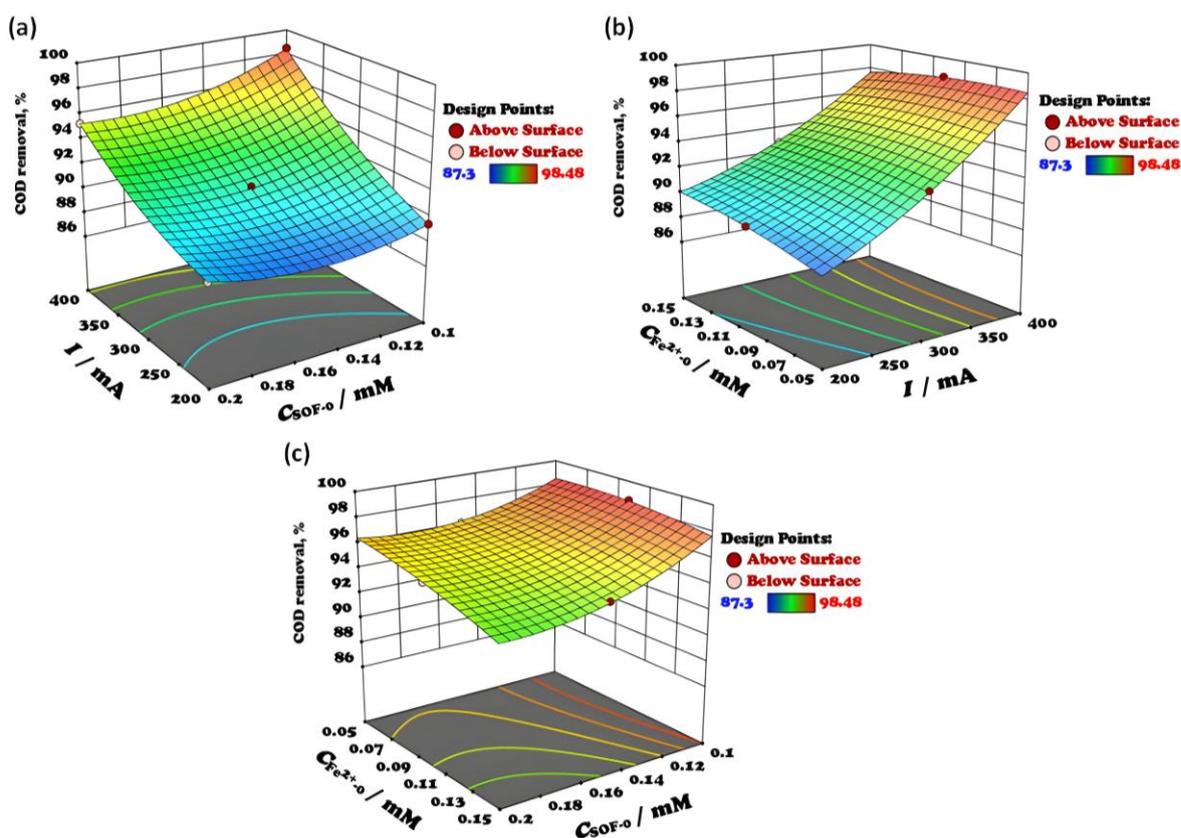

Figure 7. *3D response surface of COD removal as a function of variable pairs, with the third factor held at its optimal value, including (a) I and C_{SOF-0}; (b) I and $C_{Fe^{2+}-0}$; (c) C_{SOF-0} and $C_{Fe^{2+}-0}$*

The observed trends align with the classical approach while offering a more comprehensive view across the studied conditions. The interaction between current intensity and C_{SOF-0}, with $C_{Fe^{2+}-0}$ kept at 0.1 mM, is depicted in the 3D surface response in Figure 7a. The interaction shows that increasing current intensity improves COD removal, particularly at C_{SOF-0} = 0.1 mM, while higher concentrations reduce efficiency due to by-product formation.

Further analysis of the interaction between the applied current and $C_{Fe^{2+}-0}$, while keeping C_{SOF-0} fixed at its optimal value of 0.1 mM, provides additional insights, as the response surface in Figure 7b indicates that COD removal is primarily influenced by current intensity, with minimal impact from $C_{Fe^{2+}-0}$ beyond 0.1 mM. Moreover, Figure 7c confirms that optimal conditions are achieved at 0.1 mM for both SOF and Fe^{2+}, reinforcing the importance of precise parameter adjustments in the EF process.

Model-based optimization of operating conditions

The desirability function (DF), ranging from 0 (undesirable) to 1 (highly desirable), was used to optimize SOF mineralization. As depicted in Figure 8, the *DF* evaluates the effect of key variables on COD removal efficiency and identifies the optimal conditions for the system.
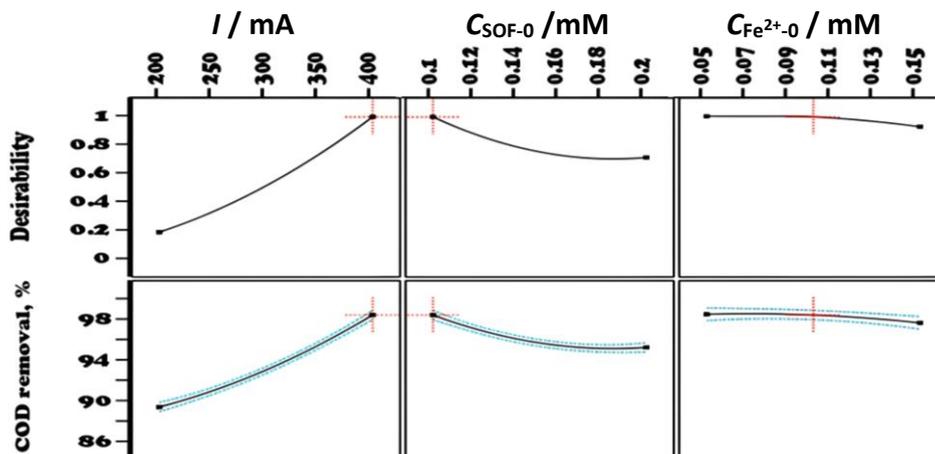

Figure 8. *Profiles for predicated values and desirability function for SOF removal via the EF process*

The maximum DF value highlights the most effective settings for the variables studied, as illustrated in the response values and desirability profile. The three parameters (*i.e. I*, C_{SOF-0}, and $C_{Fe^{2+}-0}$) were set 'in range', while the COD removal efficiency was set to 'maximize' (Table 8). Additionally, the lower and upper limits for COD removal were taken from the BBD levels, with the objective of enhancing the removal efficiency.

Table 8. *Parameter constraints and optimization goals for COD removal efficiency*

Name	Goal	Lower limit	Upper limit
I / mA	is in range	200	400
C_{SOF-0} / mM	is in range	0.1	0.2
$C_{Fe^{2+}-0}$ / mM	is in range	0.05	0.15
COD removal, %	maximize	87.3	98.5

The ideal conditions for achieving maximum COD removal were found to be *I* = 400 mA, C_{SOF-0} = 0.1 mM and $C_{Fe^{2+}-0}$ ranging from 0.05 and 0.1 mM, achieving a desirability score of 1. At 400 mA, the maximum COD removal of 98.5 % was recorded, whereas lower currents led to reduced efficiency and desirability. The initial SOF concentration of 0.1 mM was also optimal, with higher concentrations causing a gradual decline in both COD removal and desirability. For Fe^{2+} concentration, the ideal range was between 0.05 and 0.1 mM, which produced the best results for mineralization. The desirability function effectively identified these optimal conditions, ensuring maximum COD removal and efficient SOF treatment. Additionally, the experimental results, showing a 98.5 % removal of SOF, align with the COD removal of 98.5 % predicted by the quadratic model, validating the model's accuracy and reliability in predicting SOF mineralization outcomes.

Bio-electro-Fenton process

Evaluation of the biodegradability

The evolution of SOF solution biodegradability during EF treatment under optimal conditions was evaluated by the BOD_5/COD ratio, which reflects the proportion of organic matter susceptible to biodegradation. A rise in this ratio indicates enhanced biodegradability, with a value of 0.40

sometimes considered a threshold for a solution to be classified as readily biodegradable [27,66,67]. To evaluate the EF process as a pre-treatment and determine the optimal time for coupling with biological treatment as a post-treatment for complete mineralization at a reasonable cost, BOD_5 measurements were conducted before and after electrolysis. Figure 9 illustrates the progression of COD removal and the BOD_5/COD ratio over time of electrochemical pre-treatment.
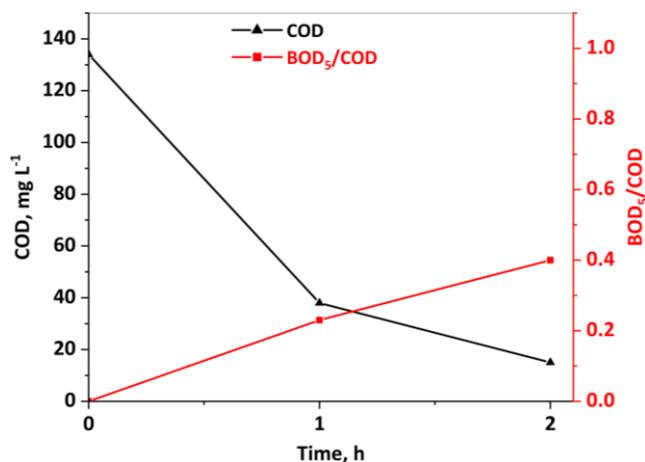

Figure 9. *Evolution of COD removal and BOD_5/COD ratio during SOF treatment via EF process at pH 3±0.1; I = 400 mA; C_{SOF-0} = 0.1 mM; $C_{Fe^{2+}-0}$ = 0.1 mM; $C_{Na_2SO_4}$ = 0.05 M; V_s = 200 mL*

Before electrolysis, SOF was non-biodegradable, as indicated by the BOD_5/COD ratio <0.02, highlighting the need for pre-treatment before biological treatment. After 1 h of electrolysis, biodegradability already significantly improved, with a BOD_5/COD ratio of 0.23. After 2 h, the solution became readily biodegradable, achieving a ratio of 0.41. This enhancement is likely due to the oxidation of persistent SOF molecules by $^\bullet$OH and conversion into more easily biodegradable byproducts [56,68]. Final by-products in the solution at 2 h were more biodegradable than the initial byproducts obtained at 1 h. It may be attributed to a higher proportion of easily biodegradable byproducts, such as short-chain carboxylic acids. The results demonstrate that partial removal of the COD by the EF process might be sufficient, while the subsequent biological treatment step (bio-EF) to complete the mineralization process might allow for achieving a high overall COD removal [17,24,27].

Biological aerobic treatment by activated sludge

The choice of a 2-hour EF treatment at 400 mA for the pre-treatment stage is supported by the resulting BOD_5/COD ratio of 0.41. In the combined bio-EF process, the EF treatment is intentionally stopped before complete mineralization, and the pre-treated effluent is then directed to a biological treatment. This allows the biological stage to complete the degradation of the remaining organic compounds, thereby improving overall biodegradability while reducing energy consumption compared to full EF treatment. The experiment was conducted under optimal conditions. The electrolyzed solution was subsequently treated biologically under aerobic conditions using activated sludge culture. The progress in COD removal achieved through the combined treatment is presented in Figure 10.

The results indicate that the 2-hour EF pre-treatment process resulted in 89 % mineralization, and after 18 days of culture, microorganisms were able to degrade the remaining 11 % of the initial COD. This result suggests that the intermediates formed during the electrochemical stage were highly biodegradable and compatible with subsequent biological treatment [25,27], as reflected in the increased BOD_5/COD ratio. In contrast, when a 0.1 mM SOF solution was subjected to aerobic

treatment without prior pretreatment, no detectable biodegradation occurred under the same conditions. The biological treatment alone fails to degrade SOF. It confirms the drug's lack of biodegradability, consistent with the low BOD_5/COD ratio <0.02. These results are a new indication of the effectiveness of the bio-electro-Fenton process, using the strong oxidative power of EF while participating in reducing operating cost by reducing the treatment time required for the EF step [17,33].

Although this study was conducted in ultrapure water, it does not fully represent the complexity of real wastewater. Nevertheless, sofosbuvir is an emerging micropollutant that remains insufficiently studied, and different pharmaceuticals can generate distinct transformation products with varying biodegradability.
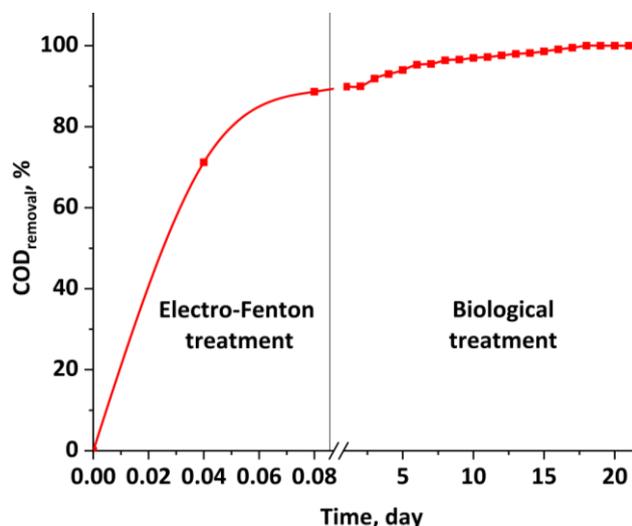

Figure 10. *Time-course of the overall COD removal during the integrated bio-electro-Fenton process at 20±1 °C, pH 7±0.2 of a pre-treated SOF solution for 2 h at pH 3±0.1; $C_{SOF-0} = 0.1$ mM; $C_{Fe^{2+}-0} = 0.1$ mM; $C_{Na_2SO_4} = 0.05$ M; I = 400 mA; $V_s = 200$ mL*

Conducting the experiments under controlled synthetic conditions allowed us to monitor its degradation pathways and assess the biodegradability of its by-products with high resolution. Considering that SOF is typically present at very low concentrations in real wastewater, initial studies under synthetic conditions are necessary to reliably track its transformation and the formation of by-products. Future work should apply the optimized EF conditions, integrate biological treatment, and extend the study to more complex matrices, potentially using heterogeneous EF, alternative electrodes, and 3D-printed cells, to develop a sustainable and scalable treatment strategy.

Conclusions

In this work, we explored the efficiency of the homogeneous EF process for degrading and mineralizing the antiviral drug SOF in aqueous medium, using a Pt anode and a CF cathode. The potential of combining this process with biological treatment was also examined. The experimental approach was designed using RSM based on the BBD to analyze three key parameters: initial SOF concentration (0.1 to 0.2 mM), initial catalyst Fe^{2+} concentration (0.05 to 0.15 mM), and applied current (100 to 500 mA). The model showed high reliability, with an R^2 value of 0.99, and the optimal conditions were determined to be an initial SOF concentration of 0.1 mM, an initial catalyst concentration between 0.05 and 0.1 mM, and a current intensity of 400 mA. These results were validated with a more traditional experimental approach based on changing one variable at a time. Under these conditions, the process achieved complete mineralization within 5 h, with 97 %

degradation occurring within the first 5 min of electrolysis. To make the EF process more cost-effective for mineralization, it was combined with a biological treatment. Biodegradability tests under optimal conditions showed an increase in the BOD_5/COD ratio to 0.41 after 2 h of electrolysis, indicating that the solution became biodegradable. The EF process was applied as a 2-hour pre-treatment, followed by a batch biological treatment using activated sludge as a post-treatment. This combined method achieved complete mineralization of the solution. These findings are a new indication of the potential of the bio-electro-Fenton process for achieving full mineralization of recalcitrant organic compounds in a cost-effective way. Further improvements should focus on optimizing the process to enhance biodegradability within shorter treatment times, making it even more practical for large-scale applications.

References

[1]   A. Shokri, B. Nasernejad, M. Sanavi Fard, Challenges and Future Roadmaps in Heterogeneous Electro-Fenton Process for Wastewater Treatment, *Water, Air, & Soil Pollution* **234** (2023) 153. https://doi.org/10.1007/s11270-023-06139-5.

[2]   A. Shokri, K. Mahanpoor, Using UV/ZnO process for degradation of Acid red 283 in synthetic wastewater, *Bulgarian Chemical Communications* **50(1)** (2018) 27-32. https://www.researchgate.net/publication/325554795_Using_UVZnO_process_for_degradation_of_Acid_red_283_in_synthetic_wastewater.

[3]   M. Bilal, K. Rizwan, M. Adeel, H.M.N. Iqbal, Hydrogen-based catalyst-assisted advanced oxidation processes to mitigate emerging pharmaceutical contaminants, *International Journal of Hydrogen Energy* **47(45)** (2022) 19555-19569. https://doi.org/10.1016/j.ijhydene.2021.11.018.

[4]   P. Krasucka, A. Rombel, X.J. Yang, M. Rakowska, B. Xing, P. Oleszczuk, Adsorption and desorption of antiviral drugs (ritonavir and lopinavir) on sewage sludges as a potential environmental risk, *Journal of Hazardous Materials* **425** (2022) 127901. https://doi.org/10.1016/j.jhazmat.2021.127901.

[5]   K. Kümmerer, Pharmaceuticals in the environment, *Annual Review of Environment and Resources* **35** (2010) 57-75. https://doi.org/10.1146/annurev-environ-052809-161223.

[6]   E. De Clercq, P. Herdewijn, *Strategies in the design of antiviral drugs*, in *Pharmaceutical Sciences Encyclopedia,* S.C. Gad (Ed.), Wiley, 2010, pp. 1-56. https://doi.org/10.1002/9780470571224.pse026.

[7]   E. De Clercq, Three decades of antiviral drugs, *Nature Reviews Drug Discovery* **6(12)** (2007) 941-941. https://doi.org/10.1038/nrd2485.

[8]   A.C. Singer, M.A. Nunn, E.A. Gould, A.C. Johnson, Potential risks associated with the proposed widespread use of Tamiflu, *Environmental Health Perspectives* **115(1)** (2007) 102-106. https://doi.org/10.1289/ehp.9574.

[9]   O. Mitjà, B. Clotet, Use of antiviral drugs to reduce COVID-19 transmission, *The Lancet Global Health* **8(5)** (2020) e639-e640. https://doi.org/10.1016/S2214-109X(20)30114-5.

[10]   P. Mishra, J. Florian, K. Qi, W. Zeng, L.K. Naeger, E. Donaldson, S. Connelly, J. O'Rear, D. Price, J. Murray, et al., FDA perspective on sofosbuvir therapy for patients with chronic hepatitis C virus genotype 1 infection who did not respond to treatment with pegylated interferon and ribavirin, *Gastroenterology* **147(6)** (2014) 1196-1200. https://doi.org/10.1053/j.gastro.2014.10.027.

[11]   C. Prasse, M. P. Schlüsener, R. Schulz, T. A. Ternes, Antiviral drugs in wastewater and surface waters: a new pharmaceutical class of environmental relevance?, *Environmental Science & Technology* **44(5)** (2010) 1728-1735. https://doi.org/10.1021/es903216p.

[12]   H. Babas, G. Kaichouh, M. Khachani, M. E. Karbane, A. Chakir, A. Guenbour, A. Bellaouchou, I. Warad, A. Zarrouk, Equilibrium and kinetic studies for removal of antiviral sofosbuvir from aqueous solution by adsorption on expanded perlite: Experimental, modelling and opti-mization, *Surfaces and Interfaces* **23** (2021) 100962. https://doi.org/10.1016/j.surfin.2021.100962.

[13]   A. Shokri, Photocatalytic Degradation of Nitrotoluene in Synthetic Wastewater by $CoFe_2O_4/SiO_2/TiO_2$ Nanoparticles Using Box-Behnken Experimental Design, *Desalination and Water Treatment* **247** (2022) 92-99. https://doi.org/10.5004/dwt.2022.28037.

[14]   W.H. Glaze, J.-W. Kang, D.H. Chapin, The chemistry of water treatment processes involving ozone, hydrogen peroxide and ultraviolet radiation, *Ozone: Science & Engineering* **9(4)** (1987) 335-352. https://doi.org/10.1080/01919518708552148.

[15]   A. Shokri, Employing UV/Peroxydisulphate (PDS) Activated by Ferrous Ion for the Removal of Toluene in Aqueous Environment: Electrical Consumption and Kinetic Study, *International Journal of Environmental Analytical Chemistry* **102** (2022) 4478-4495. https://doi.org/10.1080/03067319.2020.1784887.

[16]   S. Mohammadi, M. Zarei, M.S. Amini-Fazl, M. Ebratkhahan, Removal and mineralization of prednisolone from water by using homogeneous and heterogeneous electro-Fenton processes, *Journal of Environmental Chemical Engineering* **11(5)** (2023) 110465. https://doi.org/10.1016/j.jece.2023.110465.

[17]   N. Oturan, M.A. Oturan, Electro-Fenton process: background, new developments, and applications, in *Electrochemical Water and Wastewater Treatment*, Elsevier, 2018, pp. 193-221. https://doi.org/10.1016/B978-0-12-813160-2.00008-0.

[18]   C. Trellu, Y. Péchaud, N. Oturan, E. Mousset, D. Huguenot, E.D. Van Hullebusch, G. Esposito, M.A. Oturan, Comparative study on the removal of humic acids from drinking water by anodic oxidation and electro-Fenton processes: mineralization efficiency and modelling, *Applied Catalysis B* **194** (2016) 32-41. https://doi.org/10.1016/j.apcatb.2016.04.039.

[19]   A. Bayat, A. Shokri, Degradation of P-Nitrotoluene in Aqueous Environment by Fe(II)/Peroxymonosulfate Using Full Factorial Experimental Design, *Separation Science and Technology* **56(17)** (2021) 2941-2950 https://doi.org/10.1080/01496395.2020.1861016.

[20]   A. Shokri, B. Nasernejad, Investigation of Spent Caustic Effluent Treatment by Electro-Peroxone Process; Cost Evaluation and Kinetic Studies, *Journal of Industrial and Engineering Chemistry* **129** (2024) 170-179 https://doi.org/10.1016/j.jiec.2023.08.030.

[21]   I. Sirés, E. Brillas, M.A. Oturan, M.A. Rodrigo, M. Panizza, Electrochemical advanced oxidation processes: today and tomorrow, *Environmental Science and Pollution Research* **21(14)** (2014) 8336-8367. https://doi.org/10.1007/s11356-014-2783-1.

[22]   E. Brillas, Progress of homogeneous and heterogeneous electro-Fenton treatments of antibiotics in synthetic and real wastewaters. A critical review on the period 2017-2021, *Science of the Total Environment* **819** (2022) 153102. https://doi.org/10.1016/j.scitotenv.2022.153102.

[23]   M.A. Oturan, An ecologically effective water treatment technique using electrochemically generated hydroxyl radicals for *in situ* destruction of organic pollutants: application to

herbicide 2,4-D, *Journal of Applied Electrochemistry* **30(4)** (2000) 475-482. https://doi.org/10.1023/A:1003994428571.

[24] E. Brillas, I. Sirés, M.A. Oturan, Electro-Fenton process and related electrochemical technologies based on Fenton's reaction chemistry, *Chemical Reviews* **109(12)** (2009) 6570-6631. https://doi.org/10.1021/cr900136g.

[25] H. Olvera-Vargas, C. Trellu, N. Oturan, M.A. Oturan, Bio-electro-Fenton: a new combined process - principles and applications, in *Electro-Fenton Process*, The Handbook of Environmental Chemistry, M. Zhou, M.A. Oturan, I. Sirés (Eds.), Springer, Singapore, 2017, Vol. 61, pp. 29-56. https://doi.org/10.1007/698_2017_53.

[26] O. Ganzenko, D. Huguenot, E. D. Van Hullebusch, G. Esposito, M. A. Oturan, Electrochemical advanced oxidation and biological processes for wastewater treatment: a review of the combined approaches, *Environmental Science and Pollution Research* **21(14)** (2014) 8493-8524. https://doi.org/10.1007/s11356-014-2770-6.

[27] H. Olvera-Vargas, T. Cocerva, N. Oturan, D. Buisson, M.A. Oturan, Bioelectro-Fenton: a sustainable integrated process for removal of organic pollutants from water: application to mineralization of metoprolol, *Journal of Hazardous Materials* **319** (2016) 13-23. https://doi.org/10.1016/j.jhazmat.2015.12.010.

[28] H. Khan, S. Hussain, M.A. Ud Din, M. Arshad, F. Wahab, U. Hassan, A. Khan, Multiple design and modelling approaches for the optimisation of carbon felt electro-Fenton treatment of dye laden wastewater, *Chemosphere* **338** (2023) 139510. https://doi.org/10.1016/j.chemosphere.2023.139510.

[29] H. Liu, X.Z. Li, Y.J. Leng, C. Wang, Kinetic modeling of electro-Fenton reaction in aqueous solution, *Water Research* **41(5)** (2007) 1161-1167. https://doi.org/10.1016/j.watres.2006.12.006.

[30] L. Carelle, L. Waffo, J. Marie, J.M. Dangwang Dikdim, G. Noumi, J. Sieliechi, A. Guessous, F. Echerfaoui, M. El Karbane, I. Warad, et al., Investigation on tenofovir removal from water by electro-Fenton process: optimization of the mineralization using Box-Behnken design, *Biointerface Research in Applied Chemistry* **13(6)** (2023) 522. https://doi.org/10.33263/BRIAC136.522.

[31] A. Özcan, Y. Şahin, A.S. Koparal, M.A. Oturan, Propham mineralization in aqueous medium by anodic oxidation using boron-doped diamond anode: influence of experimental parameters on degradation kinetics and mineralization efficiency, *Water Research* **42(12)** (2008) 2889-2898. https://doi.org/10.1016/j.watres.2008.02.027.

[32] I. Yahiaoui, F. Aissani-Benissad, F. Fourcade, A. Amrane, Removal of tetracycline hydrochloride from water based on direct anodic oxidation (Pb/PbO$_2$ electrode) coupled to activated sludge culture, *Chemical Engineering Journal* **221** (2013) 418-425. https://doi.org/10.1016/j.cej.2013.01.091.

[33] L. Rachidi, A. Guessous, I. Haji, M. El Karbane, H. Chakchak, A. Zouhir, A. Talidi, I. Warad, A. Zarrouk, G. Kaichouh, Combined electro-Fenton and biological process for treatment of antidepressant sertraline: performance enhancement and by-products monitoring, *Analytical & Bioanalytical Electrochemistry* **15(6)** (2023) 458-473. https://doi.org/10.22034/abec.2023.705726.

[34] F. Ferrag-Siagh, F. Fourcade, I. Soutrel, H. Aït-Amar, H. Djelal, A. Amrane, Tetracycline degradation and mineralization by the coupling of an electro-Fenton pretreatment and a biological process, *Journal of Chemical Technology and Biotechnology* **88(7)** (2013) 1380-1386. https://doi.org/10.1002/jctb.3990.

[35] J. Li, T. Tao, X. Li, J. Zuo, T. Li, J. Lu, S. Li, L. Chen, C. Xia, Y. Liu, et al., A spectrophotometric method for determination of chemical oxygen demand using home-made reagents, *Desalination* **239(1-3)** (2009) 139-145. https://doi.org/10.1016/j.desal.2008.03.014.

[36]   W. Liu, Z. Ai, L. Zhang, Design of a neutral three-dimensional electro-Fenton system with foam nickel as particle electrodes for wastewater treatment, *Journal of Hazardous Materials* **243** (2012) 257-264. https://doi.org/10.1016/j.jhazmat.2012.10.024.

[37]   K. He, X. Guo, G. Wang, J. Xiong, H. Peng, F. Lai, J. He, Excellent treatment effect of actual wastewater from a pesticide plant using electro-Fenton process catalyzed by natural pyrite, *Journal of Environmental Chemical Engineering* **11(6)** (2023) 111211. https://doi.org/10.1016/j.jece.2023.111211.

[38]   Ş. Camcıoğlu, B. Özyurt, N. Oturan, D. Portehault, C. Trellu, M.A. Oturan, Heterogeneous electro-Fenton treatment of chemotherapeutic drug busulfan using magnetic nanocomposites as catalyst, *Chemosphere* **341** (2023) 140129. https://doi.org/10.1016/j.chemosphere.2023.140129.

[39]   K. Cruz-González, O. Torres-López, A. García-León, J.L. Guzmán-Mar, L.H. Reyes, A. Hernández-Ramírez, J.M. Peralta-Hernández, Determination of optimum operating parameters for Acid Yellow 36 decolorization by electro-Fenton process using BDD cathode, *Chemical Engineering Journal* **160(1)** (2010) 199-206. https://doi.org/10.1016/j.cej.2010.03.043.

[40]   B.K. Körbahti, Response surface optimization of electrochemical treatment of textile dye wastewater, *Journal of Hazardous Materials* **145(1-2)** (2007) 277-286. https://doi.org/10.1016/j.jhazmat.2006.11.031.

[41]   S.Y. Guvenc, H.S. Erkan, G. Varank, M.S. Bilgili, G.O. Engin, Optimization of paper mill industry wastewater treatment by electrocoagulation and electro-Fenton processes using response surface methodology, *Water Science and Technology* **76(8)** (2017) 2015-2031. https://doi.org/10.2166/wst.2017.327.

[42]   M. Panizza, M.A. Oturan, Degradation of Alizarin Red by electro-Fenton process using a graphite-felt cathode, *Electrochimica Acta* **56(20)** (2011) 7084-7087. https://doi.org/10.1016/j.electacta.2011.05.105.

[43]   A. Wang, J. Qu, J. Ru, H. Liu, J. Ge, Mineralization of an azo dye Acid Red 14 by electro-Fenton's reagent using an activated carbon fiber cathode, *Dyes and Pigments* **65(3)** (2005) 227-233. https://doi.org/10.1016/j.dyepig.2004.07.019.

[44]   N. Oturan, M. Panizza, M.A. Oturan, Cold incineration of chlorophenols in aqueous solution by advanced electrochemical process electro-Fenton. Effect of number and position of chlorine atoms on the degradation kinetics, *The Journal of Physical Chemistry A* **113(41)** (2009) 10988-10993. https://doi.org/10.1021/jp9069674.

[45]   A.R. Rahmani, D. Nematollahi, G. Azarian, K. Godini, Z. Berizi, Activated sludge treatment by electro-Fenton process: parameter optimization and degradation mechanism, *Korean Journal of Chemical Engineering* **32(8)** (2015) 1570-1577. https://doi.org/10.1007/s11814-014-0362-2.

[46]   S. Trabelsi, N. Oturan, N. Bellakhal, M. Oturan, Electrochemical oxidation of phthalic anhydride in aqueous medium by electro-Fenton process, *Journal of Environmental Engineering and Management* **19(5)** (2009) 291-297. https://www.researchgate.net/publication/228725489_Electrochemical_oxidation_of_phtalic_anhydride_in_aqueous_medium_by_electro-Fenton_process.

[47]   B. Balci, N. Oturan, R. Cherrier, M.A. Oturan, Degradation of atrazine in aqueous medium by electrocatalytically generated hydroxyl radicals. A kinetic and mechanistic study, *Water Research* **43(7)** (2009) 1924-1934. https://doi.org/10.1016/j.watres.2009.01.021.

[48]   L. Rachidi, G. Kaichouh, M. Khachani, A. Zarrouk, M.E. Karbane, H. Chakchak, I. Warad, A.E. Hourch, K.E. Kacemi, A. Guessous, Optimization and modeling of the electro-Fenton process for treatment of sertraline hydrochloride: mineralization efficiency, energy cost

and biodegradability enhancement, *Chemical Data Collections* **35** (2021) 100764. https://doi.org/10.1016/j.cdc.2021.100764.

[49]   E. Mousset, Y. Pechaud, N. Oturan, M.A. Oturan, Charge transfer/mass transport competition in advanced hybrid electrocatalytic wastewater treatment: development of a new current efficiency relation, *Applied Catalysis B: Environmental* **240** (2019) 102-111. https://doi.org/10.1016/j.apcatb.2018.08.055.

[50]   R.T. Doumbi, G. Bertrand Noumi, B. Ngobtchok, Domga, Tannery wastewater treatment by electro-Fenton and electro-persulfate processes using graphite from used batteries as free-cost electrode materials, *Case Studies in Chemical and Environmental Engineering* **5** (2022) 100190. https://doi.org/10.1016/j.cscee.2022.100190.

[51]   A. Fernandes, M.J. Nunes, A.S. Rodrigues, M.J. Pacheco, L. Ciríaco, A. Lopes, Electro-persulfate processes for the treatment of complex wastewater matrices: present and future, *Molecules* **26(16)** (2021) 4821. https://doi.org/10.3390/molecules26164821.

[52]   H. Nadais, X. Li, N. Alves, C. Couras, H.R. Andersen, I. Angelidaki, Y. Zhang, Bio-electro-Fenton process for the degradation of non-steroidal anti-inflammatory drugs in wastewater, *Chemical Engineering Journal* **338** (2018) 401-410. https://doi.org/10.1016/j.cej.2018.01.014.

[53]   L. Feng, W. Song, N. Oturan, M. Karbasi, E.D. Van Hullebusch, G. Esposito, S. Giannakis, M.A. Oturan, Electrochemical oxidation of naproxen in aqueous matrices: elucidating the intermediates' eco-toxicity, by assessing its degradation pathways via experimental and density functional theory (DFT) approaches, *Chemical Engineering Journal* **451** (2023) 138483. https://doi.org/10.1016/j.cej.2022.138483.

[54]   M. Yahya, M. El Karbane, N. Oturan, K. El Kacemi, M.A. Oturan, Mineralization of the antibiotic levofloxacin in aqueous medium by electro-Fenton process: kinetics and intermediate products analysis, *Environmental Technology* **37(10)** (2016) 1276-1287. https://doi.org/10.1080/09593330.2015.1111427.

[55]   H. Gallard, J. De Laat, B. Legube, Spectrophotometric study of the formation of iron(III)-hydroperoxy complexes in homogeneous aqueous solutions, *Water Research* **33(13)** (1999) 2929-2936. https://doi.org/10.1016/S0043-1354(99)00007-X.

[56]   C. Annabi, F. Fourcade, I. Soutrel, F. Geneste, D. Floner, N. Bellakhal, A. Amrane, Degradation of enoxacin antibiotic by the electro-Fenton process: optimization, biodegradability improvement and degradation mechanism, *Journal of Environmental Management* **165** (2016) 96-105. https://doi.org/10.1016/j.jenvman.2015.09.018.

[57]   H. Lin, J. Wu, N. Oturan, H. Zhang, M.A. Oturan, Degradation of artificial sweetener saccharin in aqueous medium by electrochemically generated hydroxyl radicals, *Environmental Science and Pollution Research* **23(5)** (2016) 4442-4453. https://doi.org/10.1007/s11356-015-5633-x.

[58]   H. Lin, N. Oturan, J. Wu, H. Zhang, M.A. Oturan, Cold incineration of sucralose in aqueous solution by electro-Fenton process, *Separation and Purification Technology* **173** (2017) 218-225. https://doi.org/10.1016/j.seppur.2016.09.028.

[59]   A. Özcan, Y. Şahin, A.S. Koparal, M.A. Oturan, Degradation of picloram by the electro-Fenton process, *Journal of Hazardous Materials* **153(1-2)** (2008) 718-727. https://doi.org/10.1016/j.jhazmat.2007.09.015.

[60]   A. Adachi, F. El Ouadrhiri, E.A.M. Saleh, R.H. Althomali, A.F. Kassem, E.M. Ibtissam, M.M. Moharam, K. Husain, N. Eloutassi, A. Lahkimi, Iron-doped catalyst synthesis in heterogeneous Fenton-like process for dye degradation and removal: optimization using response surface methodology, *SN Applied Sciences* **5(12)** (2023) 342. https://doi.org/10.1007/s42452-023-05543-0.

[61]   P. Pourali, M. Fazlzadeh, M. Aaligadri, A. Dargahi, Y. Poureshgh, B. Kakavandi, Enhanced three-dimensional electrochemical process using magnetic recoverable of Fe_3O_4@GAC towards furfural degradation and mineralization, *Arabian Journal of Chemistry* **15(8)** (2022) 103980. https://doi.org/10.1016/j.arabjc.2022.103980.

[62]   P.K. Singa, N. Rajamohan, M.H. Isa, C.Z.A. Abidin, A.H. Ibrahim, Remediation of carcinogenic PAHs from landfill leachate by electro-Fenton process - optimization and modeling, *Chemosphere* **359** (2024) 142248. https://doi.org/10.1016/j.chemosphere.2024.142248.

[63]   A. Long, H. Zhang, Selective oxidative degradation of toluene for the recovery of surfactant by an electro/Fe^{2+}/persulfate process, *Environmental Science and Pollution Research* **22(15)** (2015) 11606-11616. https://doi.org/10.1007/s11356-015-4406-x.

[64]   S.Y. Guvenc, G. Varank, Box-Behnken design optimization of electro-Fenton/persulfate processes following the acidification for TSS removal from biodiesel wastewater, *Sigma Journal of Engineering and Natural Sciences*, **38(4)** (2020) 1767-1780. https://dergipark.org.tr/en/pub/sigma/issue/65287/1004983#article_cite.

[65]   L.C. Motue Waffo, J.M. Dangwang Dikdim, G.B. Noumi, Domga, R.T. Teguia Doumbi, G. Kaichouh, J.M. Sieliechi, I. Haji, A. Guessous, M. El Karbane, Electrochemical production of sulfate radicals for degradation of tenofovir in aqueous solution, *Case Studies in Chemical and Environmental Engineering* **6** (2022) 100235. https://doi.org/10.1016/j.cscee.2022.100235.

[66]   V. Sarria, S. Parra, N. Adler, P. Péringer, N. Benitez, C. Pulgarin, Recent developments in the coupling of photoassisted and aerobic biological processes for the treatment of biorecalcitrant compounds, *Catalysis Today* **76(2-4)** (2002) 301-315. https://doi.org/10.1016/S0920-5861(02)00228-6.

[67]   J.L. De Morais, P.P. Zamora, Use of advanced oxidation processes to improve the biodegradability of mature landfill leachates, *Journal of Hazardous Materials* **123(1-3)** (2005) 181-186. https://doi.org/10.1016/j.jhazmat.2005.03.041.

[68]   D. Mansour, F. Fourcade, N. Bellakhal, M. Dachraoui, D. Hauchard, A. Amrane, Biodegradability improvement of sulfamethazine solutions by means of an electro-Fenton process, *Water, Air, & Soil Pollution* **223(5)** (2012) 2023-2034. https://doi.org/10.1007/s11270-011-1002-7.